Int. J. Heat Mass Transfer. Vol. 36, No. 16, pp. 3877–3885, 1993
Printed in Great Britain

0017–9310/93 $6.00 + 0.00

Numerical study of liquid film cooling in a turbulent gas stream

WEI-MON YAN
Department of Mechanical Engineering, Hua Fan Institute of Technology, Shih Ting, Taipei, Taiwan 22305, R.O.C.

and

CHYI-YEOU SOONG
Department of Aeronautical Engineering, Chung Cheng Institute of Technology, Taoyuan, Taiwan 33509, R.O.C.

(*Received* 23 *December* 1992 *and in final form* 10 *May* 1993)

Abstract—A numerical method for analyzing liquid film cooling along an inclined plate in a turbulent stream of air is presented. Heat and mass transfer characteristics in an air–water system are mainly considered. A marching procedure is employed for solutions of the equations of mass, momentum, energy and concentration in the system. The effects of the inclined angle ϕ, free-stream temperature T_∞, free-stream velocity u_∞, and inlet film thickness δ on the heat and mass transfer along the gas–liquid interface are examined in detail. Results show that an increase in free-stream temperature or velocity may cause a reduction in interfacial temperature, while an increase in inclined angle or inlet film thickness results in an increase in interfacial temperature. Additionally, a reduction in inclined angle ϕ causes an increase in interfacial temperature, which in turn leads to a larger latent heat flux and mass evaporation rate.

1. INTRODUCTION

LIQUID-FILM cooling refers to the introduction of a thin continuous liquid film onto a given surface for the purpose of protecting that wetted surface from thermal damage by a proximate hot gas stream. This technique provides a means of protecting, for example, the internal surfaces of a rocket motor from injurious effects of the hot gases. In the present study, attention is concentrated on the phenomena that characterize the convective exchange of heat and mass between a hot gas stream and a thin liquid film.

The study of the nature of the gas stream over a thin liquid film includes the investigation of such fundamental phenomena as interfacial structure and film instability [1, 2], and pressure drop in annular, two-phase flow [3]. The applications of the liquid-film cooling are generally related to high rates of heat and mass transfer between the gas stream and the liquid film and have been considered in refs. [4, 5]. Their predictions have not taken into account the details of transport processes in the boundary layer.

There has been renewed interest in the related subjects of two-phase flow pertaining to evaporation. The laminar and turbulent forced convection boundary layer type air–vapor flows over a vaporizing liquid film on a flat plate were numerically studied by Schroppel and Thiele [6]. Similar studies were conducted by Chow and his coworkers [7–9] for laminar and turbulent air flows of various humidity and superheated steam over a liquid water. Flow over a wedge with film evaporation was studied by Wu *et al.* [10]. Recently, Lin *et al.* [11] and Yan [12] investigated the influences of the wetted wall on laminar mixed convection heat transfer in vertical ducts. In their studies, the liquid film on the wetted wall was assumed to be extremely thin so that it was regarded as a boundary condition for heat and mass transfer only.

Due to the complicated couplings between momentum, heat and mass transfer in gas stream and momentum and heat transfer in the liquid film through their common interface, the studies [6–8, 10–12] just reviewed above all focused their attention on heat and mass transfer in the gas stream with the neglect of the liquid film thickness. The results thus produced are only good for the system with extremely thin film. In practical situations, however, the liquid film along the wall is of finite thickness and, therefore, the effects of the momentum and energy transports in the liquid film on the heat and mass transfer in the gas flow should be considered in the analysis [13]. The forced convection heat and mass transfer in gas stream has been treated in some studies [14–16]. In these studies the Nusselt type approximation was adopted to simplify the treatment about the transports in liquid film. Instead of employing the Nusselt type approximation, Yan [17] performed detailed analyses, including the transport processes in the gas flow and liquid film, to investigate the natural convection heat and mass transfer in a vertical pipe. It was found that as the Re_l increases, the Nusselt type approximation adopted by [14–16] becomes more questionable. Recently, the

NOMENCLATURE

A^+ damping-length constant
C_1, C_2, C_μ constants appearing in turbulent k–ε equations
c_p specific heat [J kg^{-1} K^{-1}]
c_{pa} specific heat for air [J kg^{-1} K^{-1}]
c_{pv} specific heat for water vapor [J kg^{-1} K^{-1}]
D mass diffusivity [m^2 s^{-1}]
g gravitational acceleration [m s^{-2}]
h_{fg} latent heat of vaporization [J kg^{-1}]
f_2, f_μ functions appearing in turbulent k–ε equations
h_M mass transfer coefficient
k turbulent kinetic energy [m^2 s^{-2}]
l reference length, 1.5 m
$\dot{m}_I''$ interfacial mass flux [kg s^{-1} m^{-2}]
M_a molar mass of air [kg K^{-1} mol^{-1}]
M_v molar mass of vapor [kg K^{-1} mol^{-1}]
Nu_l interfacial Nusselt number for latent heat transport, equation (16)
Nu_s interfacial Nusselt number for sensible heat transport, equation (15)
Nu_x overall Nusselt number, $Nu_s + Nu_l$, equation (13)
p_I partial pressure of water vapor at the gas–liquid interface [kPa]
Pr_t turbulent Prandtl number
p_∞ mixture pressure at the free stream [kPa]
q_I'' total interfacial energy flux in gas side [W m^{-2}]
q_{II}'' interfacial latent heat flux in gas side (or net enthalpy flux), $\dot{m}_I'' \cdot h_{fg}$ [W m^{-2}]
q_{SI}'' interfacial sensible heat flux in gas side [W m^{-2}]
q_w'' wall heat flux [W m^{-2}]
r dimensionless wall coordinate, $y \cdot u_* / \nu$
Re_l liquid film Reynolds number, $\int_0^\delta u_l \, dy/\nu$
R_t turbulent Reynolds number, $k^2/(\nu\varepsilon)$
Sh interfacial Sherwood number, equation (17)
T temperature [K, °C]
T_{li} inlet liquid film temperature [K, °C]
T_I gas–liquid interface temperature [K, °C]
T_∞ free stream temperature [K, °C]
u axial velocity [m s^{-1}]
u_∞ free stream velocity [m s^{-1}]
u_* shear stress velocity, $(\tau_w/\rho)^{1/2}$
v transverse velocity [m s^{-1}]
w mass fraction of water vapor
w_I mass fraction of vapor at gas–liquid interface
x coordinate in the flow direction [m]
X dimensionless coordinate in the flow direction, x/l
y coordinate in the transverse direction [m]
y^+ dimensionless wall coordinate, $(y-\delta_x) \cdot u_* / \nu$.

Greek symbols

δ inlet liquid film thickness [m]
δ_x local liquid film thickness [m]
ε the rate of dissipation of turbulent kinetic energy [m^2 s^{-3}]
λ molecular thermal conductivity [W m^{-1} °C^{-1}]
λ_t turbulent eddy conductivity [W m^{-1} °C^{-1}]
τ_I shear force at the gas–liquid interface [kPa]
τ_w wall shear stress [kPa]
μ molecular dynamic viscosity [N s m^{-2}]
μ_t turbulent eddy viscosity [N s m^{-2}]
ρ density [kg m^{-3}]
ϕ inclined angle of the plate
σ_k turbulent Prandtl number for k
σ_ε turbulent Prandtl number for ε.

Subscripts

a of air
I condition at the gas–liquid interface
g of mixture (air + water vapor)
l of liquid
t turbulent
v of vapor
w condition at wall
∞ condition at the inlet or free stream.

liquid film cooling along an inclined plate in a laminar gas stream was investigated by Yan and Soong [13]. Still, the liquid film cooling in a turbulent gas stream has not received sufficient attention. This motivates the present study to examine the liquid film cooling along an inclined plate in a turbulent gas stream.

2. ANALYSIS

A schematic diagram of the physical system under consideration, as shown in Fig. 1, is an inclined plate with inclined angle ϕ. The surface is exposed to a hot turbulent gas stream at free stream temperature T_∞ and velocity u_∞ and is protected by a thin water film. The liquid film is fed at inlet temperature T_{li} with film thickness δ. Heat is transferred from the hot gas to the liquid film, and the simultaneous mass transfer from the liquid film to the gas occurs as the liquid film vaporizes. The liquid film thins down along the inclined surface due to the evaporation of liquid into the hot gas stream as well as the shearing action of the hot gas stream. Note that the gas–liquid interfacial

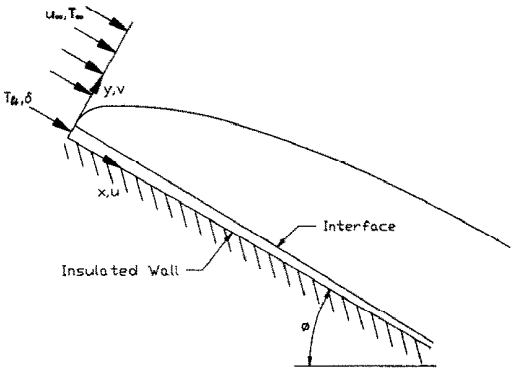

FIG. 1. Schematic diagram of the physical system.

heat and mass transfer is determined by the coupled transport processes in the gas stream and liquid film. The transport processes in the liquid film are affected by the interfacial shearing effect and vaporization at the interface. In this study, a detailed numerical analysis is performed by simultaneously solving the conservation equations for various transport processes in the liquid film and turbulent gas flow with the interfacial matching conditions treated.

2.1. *Basic equations for the liquid film*

In this work, consideration is given to a system having a sufficiently high liquid mass flow rate for which the liquid film may flow turbulently. As shown in Dukler [18], the surface waves on a falling liquid film at $Re_l > 20$ normally appear except in regions near the start of the flow. The waves have the three-dimensional and unsteady characters. Due to the complexity of the wavy motion, an assumption of the time-wise steady film thickness, which has also been used in numerous investigations [19–21], is adopted in the present study. This steady film thickness can be interpreted as the temporal average of the large amplitude waves on the surface of the actual film [20]. Additionally, to facilitate the analysis, the inertial terms in the liquid-film momentum equation are neglected as compared with the diffusion term [14–16]. In this circumstance, the boundary-layer flow in the liquid film is governed by the following conservation equations:

axial-momentum equation

$$\partial[(\mu_l+\mu_{lt})\partial u_l/\partial y]/\partial y+\rho_l g\cdot\sin\phi=0 \quad (1)$$

energy equation

$$\rho_l c_{pl} u_l \partial T_l/\partial x=\partial[(\lambda_l+\lambda_{lt})\partial T_l/\partial y]/\partial y \quad (2)$$

where μ_{lt} and λ_{lt} are the turbulent viscosity and turbulent conductivity.

2.2. *Basic equations for the gas stream*

Turbulent forced convection heat and mass transfer in the gas flow can be explored by the following equations of boundary-layer type:

continuity equation

$$\partial(\rho_g u_g)/\partial x+\partial(\rho_g v_g)/\partial y=0 \quad (3)$$

axial-momentum equation

$$\rho_g u_g\partial u_g/\partial x+\rho_g v_g\partial u_g/\partial y=\partial[(\mu_g+\mu_{gt})\partial u_g/\partial y]/\partial y \quad (4)$$

energy equation

$$\rho_g c_{pg} u_g\partial T_g/\partial x+\rho_g c_{pg} v_g\partial T_g/\partial y=\partial[(\lambda_g+\lambda_{gt})\partial T_g/\partial y]/\partial y \quad (5)$$

concentration equation of water vapor

$$\rho_g u_g\partial w/\partial x+\rho_g v_g\partial w/\partial y=\partial[\rho_g(D+D_t)\partial w/\partial y]/\partial y. \quad (6)$$

Note that the μ_{gt}, λ_{gt} and D_t are the turbulent viscosity, conductivity and mass diffusivity of the binary gas mixture, respectively. These will be modeled in Section 3.

2.3. *Boundary and interfacial matching conditions*

The two sets of governing equations, equations (1), (2) and (3)–(6), are subjected to the following boundary conditions: no-slip and adiabatic conditions are imposed at the wall, and the boundary conditions at inlet and free stream are the uniform free-stream velocity u_∞, temperature T_∞ and concentration w_∞.

The matching conditions at the gas–liquid interface, $y=\delta_x$, are given as:

1. continuity of velocity and temperature

$$u_l(x)=u_{g,I}=u_{l,I},\quad T_I(x)=T_{g,I}=T_{l,I} \quad (7)$$

2. continuity of shear stress

$$\tau_I(x)=[(\mu+\mu_t)\partial u/\partial y]_{g,I}=[(\mu+\mu_t)\partial u/\partial y]_{l,I} \quad (8)$$

3. vaporizing flux of vapor into the gas flow

$$\dot m_I''=-[\rho(D+D_t)/(1-w_I)]\partial w/\partial y \quad (9)$$

4. energy balance at the gas–liquid interface

$$[-(\lambda+\lambda_t)\partial T/\partial y]_{l,I}=[-(\lambda+\lambda_t)\partial T/\partial y]_{g,I}+\dot m_I''\cdot h_{fg}. \quad (10)$$

At the gas–liquid interface, the liquid film equations and the gas-phase equations are coupled via boundary conditions (7)–(10). While the interfacial vapor concentration and evaporating velocity can be calculated after the interfacial temperature is known [22].

$$w_I=M_v p_I/[M_a(p-p_I)+M_v p_I] \quad (11)$$

$$v_I=-[(D+D_t)/(1-w_I)]\partial w/\partial y \quad (12)$$

where p_I is the partial pressure of the water vapor at the gas–liquid interface. M_v and M_a are, respectively, the molar masses of vapor and air. By assuming that the interface is in thermodynamic equilibrium, the relation between the interfacial temperature T_I and partial pressure p_I is obtained from ref. [23].

It is worth noting that the first and second terms on the right-hand side of equation (10) represent the interfacial heat flux from the interface to the gas

stream, q''_{SI}, and the net enthalpy due to the latent heat transfer (film vaporization), q''_{II}, respectively. The term on the LHS stands for the interfacial heat flux in the liquid side and is regarded as the total interfacial heat flux $q''_I (= q''_{SI} + q''_{II})$.

The local Nusselt number at the interface, defined as

$$Nu_x = h \cdot x/k_g = q''_I \cdot x/[\lambda_g(T_I - T_\infty)], \quad (13)$$

can be written as

$$Nu_x = Nu_s + Nu_l \quad (14)$$

where Nu_s and Nu_l denote, respectively, the local Nusselt numbers for sensible and latent heat transfer, and are defined as

$$Nu_s = xq''_{SI}/[\lambda_g(T_I - T_\infty)] \quad (15)$$

and

$$Nu_l = x(\dot{m}''_I \cdot h_{fg})/[\lambda_g(T_I - T_\infty)]. \quad (16)$$

Similarly, the local Sherwood number is defined as

$$Sh = h_M x/D = x(-\partial w/\partial y)_I/(w_I - w_\infty). \quad (17)$$

Note that the variations of the thermophysical properties with temperature and mixture composition are important for the gas mixture and liquid film, and are accounted for in the computations. The complete details on the evaluation of these properties are available in Fujii *et al.* [23].

3. TURBULENCE MODELING

3.1. *Liquid film*

A note on the turbulence model for the turbulent liquid film is in order here. We have used a modified Van Driest model that was proposed by Yih and Liu [21]. The turbulent eddy viscosity is

$$\frac{\mu_{lt}}{\mu_l} = -0.5 + 0.5\{1 + 0.64r^2(\tau/\tau_w) \cdot [1 - \exp(-y(\tau/\tau_w)^{1/2}/A^+)]^2 f^2\}^{1/2} \quad \text{for } y/\delta_x < 0.6 \quad (18)$$

where

$$A^+ = 25.1, \quad f = \exp[-1.66(1 - \tau/\tau_w)], \quad r = yu*/\nu. \quad (19)$$

For $0.6 < y/\delta_x < 1.0$, the turbulent eddy viscosity for the liquid film was taken as constant and equal to its value at y/δ_x, which may be readily obtained from equation (18). The turbulent conductivity, λ_{lt}, can then be obtained by introducing the turbulent Prandtl number Pr_t,

$$\lambda_{lt} = \mu_{lt} c_{pl}/Pr_t \quad (20)$$

where the turbulent Prandtl number Pr_t is evaluated from Cebeci and Smith [24].

It should be mentioned here that the turbulence model used takes into account the effects of interfacial shear and wave [21]. Similar turbulence models were also used to simulate the heat transfer across a turbulent falling film by Hubbard *et al.* [19] and Seban and Faghri [20]. In their studies, the time-wise steady film thickness was assumed and the predicted results agreed well with the experimental results. This leads to the validity of the time-wise steady film thickness assumption in the analysis of this class of liquid–film flows.

3.2. *Gas flow*

The turbulent viscosity for the gas stream μ_t is computed in accordance with the k–ε turbulence model. Hence the transport equations for the turbulent kinetic energy and its dissipation must be included in the analysis. To procure more reliable results, a modified low-Reynolds number $k-\varepsilon$ model developed by Myong *et al.* [25, 26] is adopted to eliminate the usage of wall functions in the computations and thus to permit direct integration of the transport equations to the gas–liquid interface.

Turbulent kinetic energy equation is

$$\rho u \partial k/\partial x + \rho v \partial k/\partial y = \partial[(\mu + \mu_t/\sigma_k)\partial k/\partial y]/\partial y + \mu_t(\partial u/\partial y)^2 - \rho\varepsilon \quad (21)$$

and the rate of dissipation of turbulent kinetic energy is determined from the equation

$$\rho u \partial \varepsilon/\partial x + \rho v \partial \varepsilon/\partial y = \partial[(\mu + \mu_t/\sigma_\varepsilon)\partial \varepsilon/\partial y]/\partial y + C_1(\varepsilon/k)\mu_t(\partial u/\partial y)^2 - \rho C_2 f_2 \varepsilon^2/k \quad (22)$$

where

$$\mu_t = \rho C_\mu f_\mu k^2/\varepsilon \quad (23)$$

$$f_2 = \{1 - 2/9 \cdot \exp[-(R_t/6)^2]\}[1 - \exp(-y^+/5)]^2 \quad (24)$$

$$f_\mu = (1 + 3.45/\sqrt{R_t}) \cdot [1 - \exp(-r/70)] \quad (25)$$

$$R_t = k^2/(\nu\varepsilon), \quad y^+ = (y - \delta_x)u*/\nu, \quad u* = (\tau_w/\rho)^{1/2}. \quad (26)$$

The other empirical constants take the following values [25, 26],

$$\sigma_k = 1.4, \quad \sigma_\varepsilon = 1.3, \quad C_1 = 1.4, \quad C_2 = 1.8, \quad C_\mu = 0.09. \quad (27)$$

4. SOLUTION METHOD

The governing equations (1)–(6), (21) and (22) are solved by the finite-difference numerical method. The matching conditions imposed at the gas–liquid interface, equations (8) and (10), are approximated by using backward difference for $(\partial\psi/\partial y)_l$ and forward difference for $(\partial\psi/\partial y)_g$ with ψ denoting u or T. Therefore, the governing equations in the gas flow and liquid film can be solved simultaneously. Because the flow under consideration is a boundary-layer type, the solution for equations (1)–(6), (21) and (22) can be

marched in the downstream direction. A fully implicit numerical scheme in which the axial convective term is approximated by upwind difference and the transverse convection and diffusion terms by central difference is employed to transform the governing equations into the finite-difference equations. Each system of finite difference equations forms a tridiagonal set which can be efficiently solved by the Thomas algorithm [27].

It is noted that the thickness of the liquid film decreases with x due to the film evaporation. Therefore, during the downstream marching at each iteration, the finite-difference computational grid must comply with the variations of the liquid and gas computational domains with x. Considering the large gradient of the variables at the entrance and near gas–liquid interface, a non-uniform grid system, in both axial and transverse directions, is employed to accommodate the drastic variations of u, T and w. The grid lines are clustered together in the regions near the inlet and the gas–liquid interface. The transverse distribution of grid nodes is arranged by locating the first five nodes in the gas side within the viscous sublayer adjacent to the gas–liquid interface and expanding the rest of the grid points to the free stream using a factor of 1.04. To produce grid-independent results, several arrangements of grid points in the x and y directions were tested. It was found that the difference in the local Nusselt number Nu_x from computations using either 201×321 or 101×161 grids are always less than 1%. Accordingly, the computations involving a 101×161 grid are considered to be sufficiently accurate to describe the heat and mass transfer in the wetted wall systems. All the results presented in the next section were composed using the latter grid. To further check the numerical scheme, the results of the limiting cases of forced convection heat and mass transfer in laminar and turbulent gas stream over a wetted flat plate were examined. The present predictions agreed well with those in refs. [6, 7].

5. RESULTS AND DISCUSSION

A number of physical parameters, namely, the inlet liquid temperature T_{li}, inclined angle ϕ, free-stream temperature T_∞, inlet film thickness δ and free-stream velocity u_∞ appear in the present study. In view of the large number of parameters and of the extreme demands of the computational task, a full parametric exploration is unrealistic. Rather, the parameters were varied systematically in order to examine the key trends in the results. In what follows, the results are particularly presented for water film evaporation. The ranges of these parameters are: ϕ ranging from 0 to 90°, T_∞ from 100 to 500°C, δ from 5×10^{-4} to 10×10^{-4} m, u_∞ from 20 to 60 m s^{-1} with T_{li} fixed at 20°C. Particular attention is paid to the effects of ϕ, T_∞, δ and u_∞ on the heat and mass transfer in the film cooling problem.

Shown in Fig. 2 are the effects of various parameters on the axial distributions of the wall and interfacial temperatures. Note that the dimensionless axial coordinate X is defined as $X = x/l$, where the reference length l is selected to be 1.5 m. The results indicate that the wall and interfacial temperatures, T_w and T_I, increase monotonically in the flow direction. This feature is due to the fact that the water film absorbs sensible heat from the hot gas stream as the liquid film falls down along the inclined plate. Therefore, T_w and T_I increase as the flow goes downstream. Moreover, the curves of T_w and T_I almost coincide with each other. This implies that the temperature drop across the liquid film is negligible.

As expected, the effectiveness of protecting the wetted plate from damage by a proximate hot gas stream is relatively poor for systems with a small inclined angle ϕ or inlet liquid film thickness δ. Therefore, the higher T_w and T_I are experienced by systems with a smaller ϕ or δ as shown in Figs. 2(a) and (c). In Fig. 2(b), the higher T_w and T_I result for a higher T_∞. This is apparently due to the larger amount of sensible heat from the hot gas stream to the water film for systems having a higher T_∞. It is interesting to note in Fig. 2(b) that, even for a free-stream temperature $T_\infty = 300$°C, wall temperature is well below the boiling point of the liquid water (100°C). The change in free-stream velocity u_∞ causes noticeable effects on the variations of T_w and T_I which increase with increasing u_∞, as shown in Fig. 2(d).

Plotted in Fig. 3 are the distributions of interfacial mass fraction of water vapor along the gas–liquid interface. As shown in Figs. 2(a) and (b), the interfacial temperature T_I is higher for a smaller inclined angle ϕ or a higher free-stream temperature T_∞. Therefore, the corresponding mass fraction of water vapor is larger for systems having a smaller ϕ or a higher T_∞.

To study the relative contributions of heat transfer through the sensible and latent heat fluxes, both the interfacial sensible heat flux q''_{sI} and latent heat flux q''_{lI} in the gas side are shown in Figs. 4(a) and (b). The negative values of q''_{sI} represent that the direction of heat transfer is from the hot gas stream to the interface. It is of interest to notice that the magnitude of q''_{sI} decreases in the flow direction X. The result is a direct consequence of the gradual increase in the interfacial temperature as the water film goes downstream so that the sensible heat flux decreases in the flow direction. Moreover, the change in inclined angle ϕ has a slight influence on the axial distributions of the sensible heat flux q''_{sI}.

Next we examine the distributions of the interfacial latent heat flux in the gas side q''_{lI}. Apparently, the values of q''_{lI} are all positive, and this demonstrates that the direction of the latent heat flux is from the interface to the gas stream. This can be realized by noting that the concentration of water vapor at the interface is higher than that in the free stream. Hence, mass diffusion of water vapor takes place and liquid

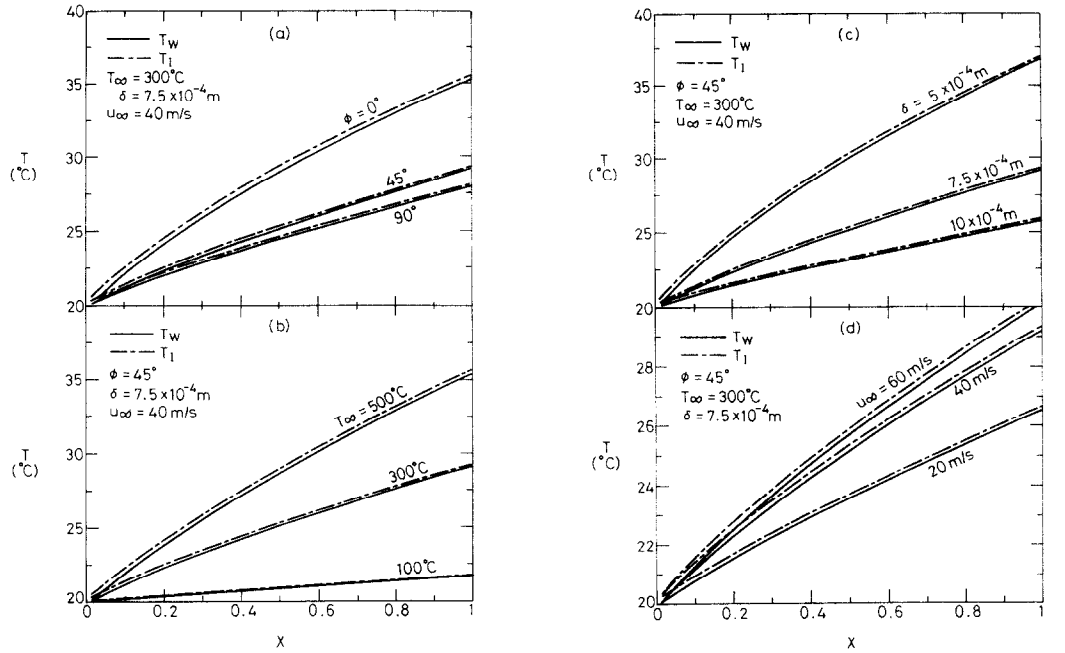

FIG. 2. Axial distributions of interfacial and wall temperatures.

water evaporates at the interface. This evaporation process absorbs a significant amount of energy ($\dot{m}_l'' \cdot h_{lg}$) through the latent heat transport. It is clearly seen in Fig. 4(b) that a system with a smaller ϕ produces a larger q_{ll}''. This is attributed to the fact that the interfacial temperature is higher when the inclined angle is smaller, which in turn causes a larger latent heat transport connected with greater film vaporization for a higher T_l. Figure 4(c) shows the distributions of the total interfacial heat flux $q_l''(=q_{sl}''+q_{ll}'')$.

To improve the understanding of the interfacial heat transfer, the longitudinal variations of the local

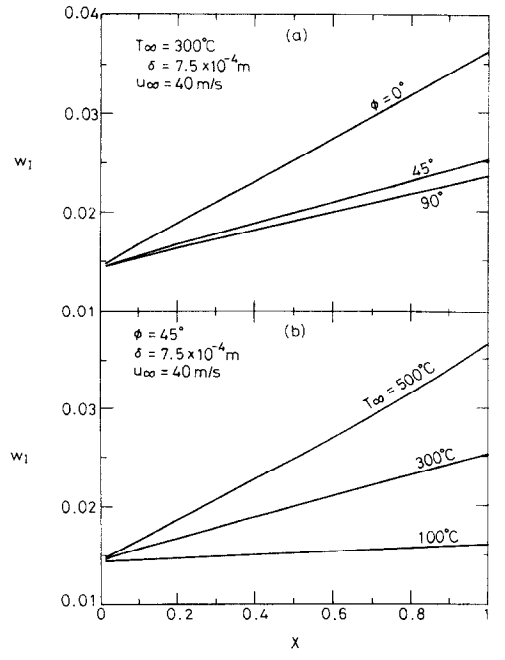

FIG. 3. Axial distributions of interfacial mass fraction.

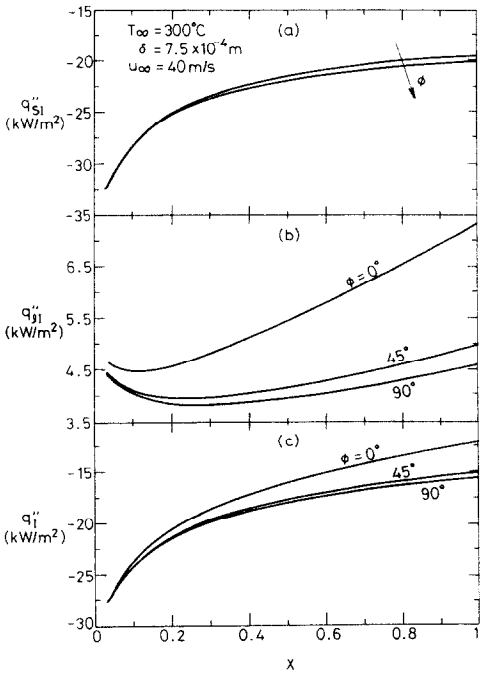

FIG. 4. Axial distributions of interfacial heat flux: (a) sensible heat flux; (b) latent heat flux; (c) overall heat flux.

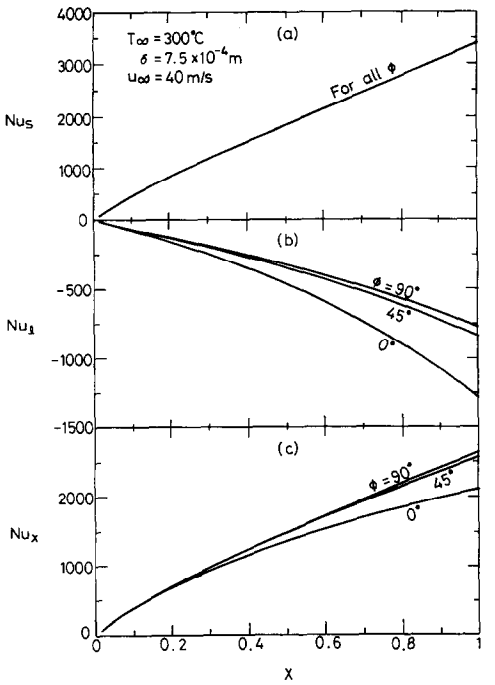

FIG. 5. Axial distributions of interfacial Nusselt number: (a) sensible heat Nusselt number; (b) latent heat Nusselt number; (c) overall Nusselt number.

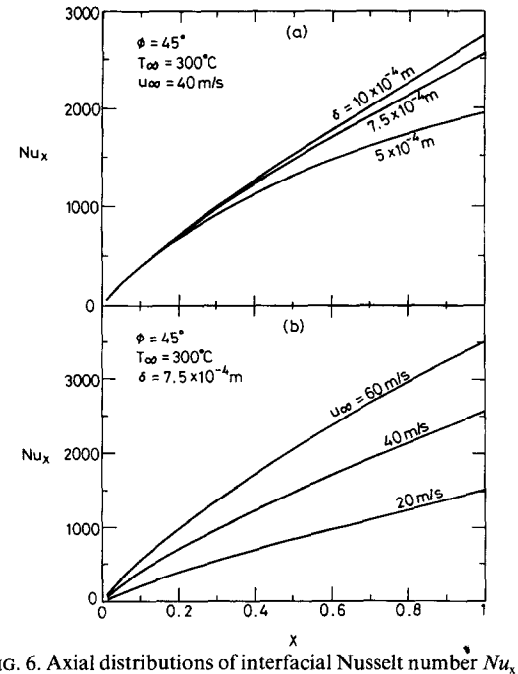

FIG. 6. Axial distributions of interfacial Nusselt number Nu_x.

Nusselt numbers for the sensible and latent heat transfer are presented in Fig. 5 for various ϕ. The negative values for Nu_l in Fig. 5(b) are resulted directly from its definition, equation (16), which is negative when $T_\infty > T_l$. In other words, negative Nu_l simply indicates that the direction of latent heat exchange is opposed to that of sensible heat exchange. This can be understood by recognizing that Nu_s, defined in equation (15), is always positive. Regarding Nu_s-curves, the curves of Nu_s for various ϕ coincide with each other. In Fig. 5(c), the total Nusselt number Nu_x ($=Nu_s+Nu_l$) is presented. It is clear that the system with a larger ϕ shows a larger Nu_x. This can be made plausible by noting that with fixed δ, the inlet liquid mass flow rate is larger for a larger ϕ. Accordingly, better heat transfer performance along the gas–liquid interface results for a system having a larger inclination.

It is interesting to investigate the influences of the inlet film thickness δ and free stream velocity u_∞ on the interfacial Nusselt number Nu_x. A larger Nu_x is noted in Fig. 6 for the systems having larger δ and u_∞, which is caused by the larger liquid flow rate or higher gas velocity near the interface.

The distributions of the interfacial mass evaporation rate and Sherwood number are presented in Fig. 7 for various ϕ to illustrate the mass transfer characteristics. A reduction in inclined angle ϕ causes a greater film evaporation due to the higher interface temperature at a smaller ϕ, as shown in Fig. 2(a). The result in Fig. 7(b) reveals that the inclined angle ϕ has only slight influence on the Sherwood number variations. The effects of the free-stream temperature and velocity on the mass transfer coefficient are of interest. Figure 8 shows that the influences of T_∞ and u_∞ on the Sh are significant.

6. CONCLUSION

A numerical analysis has been carried out to explore the detailed heat and mass transfer characteristics of

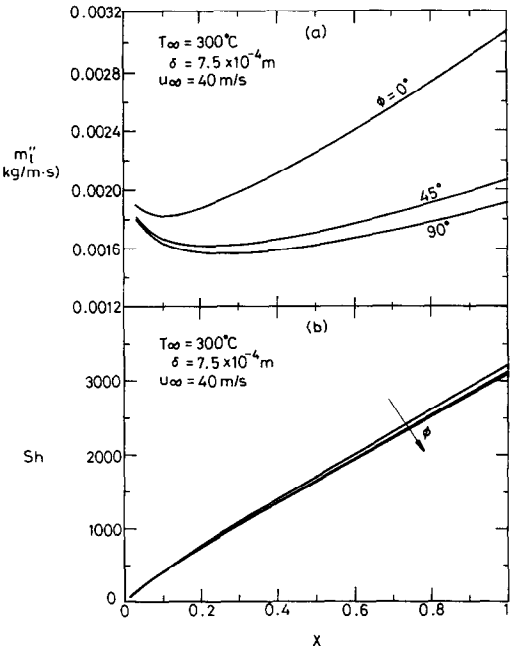

FIG. 7. Axial distributions of local mass evaporating rate and Sherwood number.

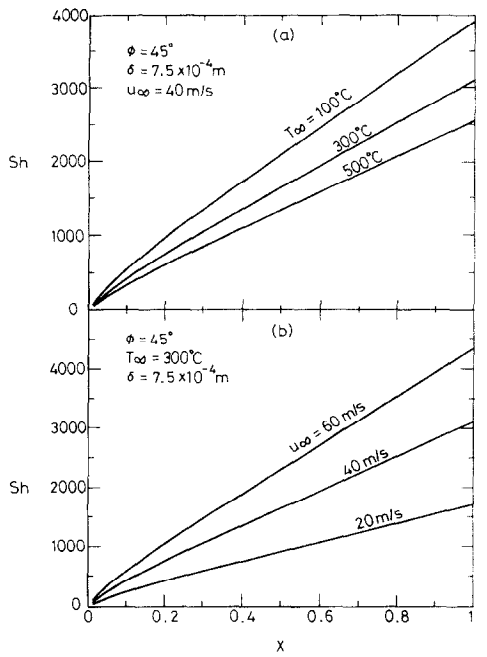

FIG. 8. Axial distributions of local Sherwood number, Sh.

the film cooling along an inclined plate by solving the respective governing equations for the liquid film and the gas stream coupled through the interfacial matching conditions. The influences of the inclined angle ϕ, free stream temperature T_∞, inlet liquid film thickness δ and free stream velocity u_∞ on the momentum, heat and mass transfer in the flow are investigated in great detail. What follows is a brief summary of the major results:

1. The interfacial temperature and water vapor concentration increase with the increasing free stream temperature T_∞ and velocity u_∞, but with decreasing inclined angle ϕ and inlet film thickness δ.

2. A reduction in inclined angle ϕ causes an increase in interfacial temperature T_1, which in turn leads to a larger latent heat flux q''_{11} and mass evaporation rate $\dot{m}''_1$.

3. Larger local Nusselt number Nu_x are experienced by systems having larger ϕ, δ and u_∞.

4. The effects of ϕ on the local mass transfer coefficient Sh are insignificant, while the effects of T_∞ and u_∞ on the Sh are considerable.

Acknowledgement—The financial support of this research by the National Science Council of R.O.C. through the contract NSC 81-0401-E014-01 is greatly appreciated.

REFERENCES

1. T. Ueda and H. Tanaka, Measurements of velocity, temperature and velocity fluctuation distributions in liquid films, *Int. J. Multiphase Flow* **2**, 261–272 (1975).
2. F. K. Wasden and A. E. Dukler, Insights into the hydrodynamics of free falling wavy films, *A.I.Ch.E. Jl* **35**, 187–195 (1989).
3. G. Zabaras, A. E. Dukler and D. Moalem-Marson, Vertical upwards cocurrent gas–liquid annular flow, *A.I.Ch.E. Jl* **32**, 829–843 (1986).
4. G. R. Kinney, A. E. Abramson and J. L. Sloop, Internal-liquid-film-cooling experiments with air-stream temperatures to 2000°F in 2- and 4-inch diameter horizontal tubes, NACA Report 1087 (1952).
5. R. A. Cater, M. L'Ecuyer and C. F. Warner, A fundamental investigation of the phenomena that characterize liquid-film cooling, NASA-CR-105906, January (1969).
6. J. Schroppel and F. Thiele, On the calculation of momentum, heat and mass transfer in laminar and turbulent boundary layer along a vaporizing liquid film, *Numer. Heat Transfer* **6**, 475–496 (1983).
7. L. C. Chow and J. N. Chung, Evaporation of water into a laminar stream of air and superheated stream, *Int. J. Heat Mass Transfer* **26**, 373–380 (1983).
8. L. C. Chow and J. N. Chung, Water evaporation into a turbulent stream of air, humid air or superheated steam, *21st ASME/A.I.Ch.E. National Heat Transfer Conference*, Seattle, WA, ASME Paper No. 83-HT-2 (1983).
9. M. Haji and L. C. Chow, Experimental measurement of water evaporation rates into air and superheated steam, *J. Heat Transfer* **110**, 237–242 (1988).
10. C. H. Wu, D. C. Davis, J. N. Chung and L. C. Chow, Simulation of wedge-shaped product dehydration using mixtures of superheated steam and air in laminar flow, *Numer. Heat Transfer* **11**, 109–123 (1987).
11. T. F. Lin, C. J. Chang and W. M. Yan, Analysis of combined buoyancy effects of thermal and mass diffusion on laminar forced convection heat transfer in a vertical tube, *J. Heat Transfer* **110**, 337–344 (1988).
12. W. M. Yan and T. F. Lin, Effect of wetted wall on laminar mixed convection in a vertical channel, *J. Thermophys. Heat Transfer* **3**, 94–96 (1988).
13. W. M. Yan and C. Y. Soong, Numerical study of liquid film cooling along an inclined plate, *Wärme- und Stoffübertragung* **28**, 233–241 (1993).
14. V. Chandra and C. W. Savery, Forced convection heat and mass transfer from a falling film to a laminar external boundary layer, *Int. J. Heat Mass Transfer* **17**, 1549–1557 (1974).
15. T. R. Shemmbharkar and B. R. Pai, Prediction of film cooling with a liquid coolant, *Int. J. Heat Mass Transfer* **29**, 899–908 (1986).
16. W. W. Baumann and F. Thiele, Heat and mass transfer in evaporating two-component liquid film flow, *Int. J. Heat Mass Transfer* **33**, 267–273 (1990).
17. W. M. Yan, The effect of liquid film vaporization on natural convection heat and mass transfer in a vertical tube, *Can. J. Chem. Engng* **70**, 452–462 (1992).
18. A. E. Dukler, Characterization, effects and modeling of the wavy gas–liquid interface, *Prog. Heat Mass Transfer* **6**, 207–234 (1972).
19. G. L. Hubbard, A. F. Mills and D. K. Chung, Heat transfer across a turbulent falling film with cocurrent vapor flow, *J. Heat Transfer* **98**, 319–320 (1976).
20. R. A. Seban and A. Faghri, Evaporation and heating with turbulent falling liquid films, *J. Heat Transfer* **98**, 315–318 (1976).
21. S. M. Yih and J. L. Liu, Prediction of heat transfer in turbulent falling liquid films with or without interfacial shear, *A.I.Ch.E. Jl* **29**, 903–909 (1983).
22. E. R. G. Eckert and R. M. Drake, Jr., *Analysis of Heat and Mass Transfer*, Chaps. 20 and 22. McGraw-Hill, New York, (1972).
23. T. Fujii, Y. Kato and K. Mihara, Expressions of transport and thermodynamic properties of air, steam and water. Sei San Ka Gaku Ken Kyu Jo., Report No. 66, Kyu Shu Dai Gaku, Kyu Shu, Japan (1977).
24. T. Cebeci and A. M. O. Smith, *Analysis of Turbulent Boundary Layer*. Academic Press, New York (1974).

25. H. K. Myong and N. Kasagi, A new approach to the improvement of k–ε turbulence model for wall bounded shear flow, *JSME Int. J.* **33,** 63–72 (1990).
26. H. K. Myong, N. Kasagi and M. Hira, Numerical prediction of turbulent pipe flow heat transfer for various Prandtl number fluids with the improved k–ε turbulence model, *JSME Int. J.* **32,** 613–622 (1990).
27. S. V. Patankar, *Numerical Heat Transfer and Fluid Flow.* Hemisphere/McGraw-Hill, New York (1980).